Pramana – J. Phys. (2017) 89:47
DOI 10.1007/s12043-017-1441-9

Impact of optical gain broadening on characteristics of response function in the presence and absence of tunnelling injection for quantum dot semiconductor lasers

YASIN YEKTA KIA and ESFANDIAR RAJAEI*

Department of Physics, Faculty of Science, University of Guilan, Rasht, Iran
*Corresponding author. E-mail: raf404@guilan.ac.ir

MS received 16 February 2017; revised 15 April 2017; accepted 27 May 2017; published online 11 September 2017

Abstract. In this paper, the dynamics of QD semiconductor lasers is investigated numerically. Large and small signal modulations for various inhomogeneous broadenings have been studied. Computationally, we have solved the rate equation for two-state InAs QD semiconductor lasers and the effect of inhomogeneous broadening on response function and output power due to variation of QD parameters have been investigated in the presence and absence of tunnelling. Also, we have studied these effects on optical gain and output power. We have shown that tunnelling injection enhances the efficiency of the semiconductor laser.

Keywords. Quantum dot; tunnelling injection; inhomogeneous; homogeneous; modulation.

PACS Nos 42.55.Px; 42.15.Eq; 42.55.Ah

1. Introduction

Quantum-dot (QD) lasers have attracted much attention due to the presence of many properties such as discrete energy states, ultralow threshold current, small temperature-insensitive operation, etc. [1–3]. These systems are more interesting due to the fact that delta-function density of state occurs in these systems leading to an interesting spectrum linewidth of QD systems. So, researchers are interested to find out the dynamical properties of QD lasers for many years.

Experimentally, the modulation bandwidth of the QD laser is lower than that of quantum well (QW) lasers [4]. In a QW, an electron in an excited state (ES) can fall to the ground state (GS) by interacting with a phonon in about 1 ps [5–7]. Phonons, having small energy, cannot transfer electron between the discrete states of QD with large energy separation. This leads to increase of relaxation time of the carriers in QD lasers. Experimental results show that carrier relaxation time is about 100 ps in InGaAs QD due to the lack of single phonon scattering and about 6 ps due to the existence of electron–hole scattering [8–10].

Tunnelling injection laser (TIL) has been suggested to enhance the modulation properties of QD lasers. In TIL design, cold carriers are injected directly from the QW layers into the active region including the QD states [11]. In this mechanism, bandwidth increases due to low concentration of carriers in the wetting layer [12]. Phonon-assisted mechanism can describe the processes of tunnelling from the QW to the QD region [13]. Experimentally, the time to tunnel from QW to QD is about a few picoseconds after considering the phonon-assisted processes [14]. Different semiconductors can be employed as a QD and a carrier injector (QW) in the TIL structures. For example, $InGaAs_{1-x}N_x$ have been used as a QW and InAs as a QD to design a TIL structure [15].

Magnetism is a very subtle issue in functionalized graphene and carbon-based materials. So, considering exciton dephasing time is a subtle issue to improve the performance of semiconductor QD lasers. In recent years, the study of homogeneous broadening has been an essential case in the literature to understand the lasing process. Exciton–phonon interaction, electron–electron interaction, and impurity scattering are responsible for the excitonic dephasing process in QDs. These scattering mechanisms depend on carrier density and temperature. As it seems, exciton–optical phonon interaction causes broadening in gain spectrum of QDs at high temperatures [16] and at low temperature the interaction between exciton and acoustic phonon is the dominant process. There is an inhomogeneous broadening

(Γ_{inhom}) of the gain spectrum in the QD lasers which is a consequence of size fluctuations in the systems [17]. The inhomogeneous broadening is chosen between 23 meV and 34 meV. The homogeneous broadening (Γ_{hom}) decreases by decreasing the temperature [18]. At low temperatures, dots contribute in the lasing process independently, while at higher temperatures, collective lasing is expected due to higher homogeneous broadening. The electron–phonon interaction can describe the temperature dependence of homogeneous linewidth. Sugawara *et al* have chosen 5 to 10 meV homogeneous broadening for ground state and 20 meV for excited state in their simulation [18–20].

Dynamical properties of tunnelling injection QD lasers were theoretically studied by considering homogeneous and inhomogeneous broadenings [21,22]. Gready *et al* have found that decrease of carrier temperature due to tunnelling narrows the homogeneous linewidth leading to the improvement of the modulation response [21]. In this paper, we obtain more dynamical properties as compared to Gready *et al* paper, considering the effect of homogeneous and inhomogeneous broadenings on dynamical properties of tunnelling injection QD lasers. In our previous work, for different carrier relaxation times, the current-output power characteristics and light emissions of the quantum-dot laser have been calculated, but we did not import the effect of tunnelling on the study of laser properties [22].

In this paper, we have investigated the effect of inhomogeneous broadening on the response function of the InGaAs/GaAs QD lasers with and without tunnelling by Runge–Kutta method. Our configurations consist of three separated WL, ES, and GS states. At first, an energy diagram for the InGaAs/GaAs QD laser is presented by considering tunnel injection. Then, we write the rate equations and calculate the modulation response of the laser. Finally, we present the simulation results to show the behaviour of output power, gain, and modulation response for small and large signal QD lasers. Our analysis gives a good understanding of the impacts of tunnelling injection on QD lasers. The capture time of carriers in TIL design with tunnelling is expected to be lower than that for QD lasers without tunnelling. Due to the lack of hot carrier distribution, the modulation properties can be improved in TIL lasing.

2. Model

In this section, we have described the rate equation of a laser with two discredit states in the presence of tunnelling. To compare the dynamical characteristics of lasing design in the presence and absence of tunnelling, we have considered different configurations.

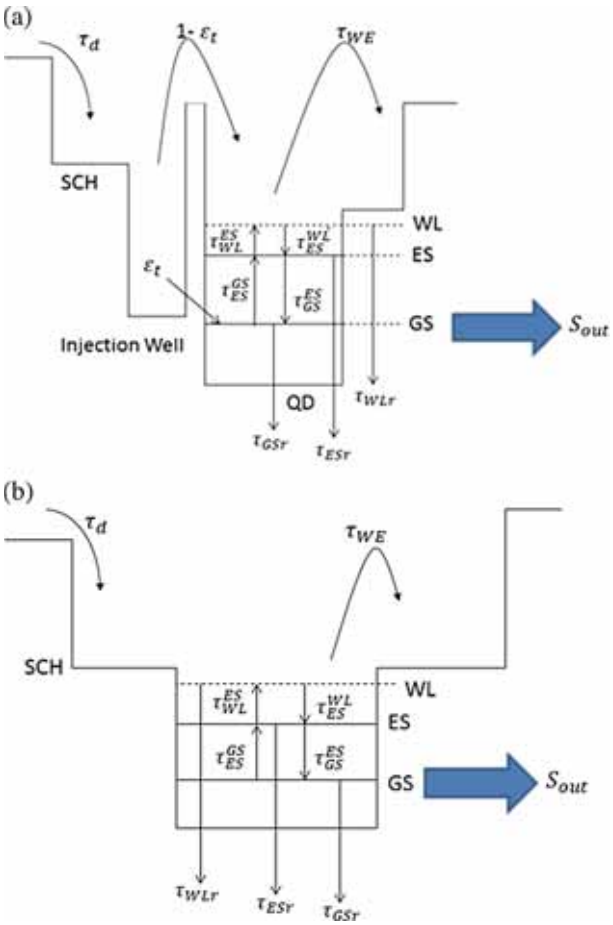

Figure 1. Schematic of carrier dynamics of a lasing system. Both carrier relaxation and escape in the couple of two discrete and two continuous levels are presented (**a**) in the presence and (**b**) in the absence of tunnelling [19].

Figure 1a illustrates a QD laser with tunnelling injection and figure 1b illustrates the case without tunnelling injection [19].

Different processes like relaxation and escape of the carriers in the two discrete and two continuous levels are presented in figure 1. QDs have a charge neutrality condition and there is no correlation between QD layers. Also, the QDs are distributed randomly in the model. The performance of QD lasers are primarily dominated by the dynamics of carriers and photons, like carrier relaxation, capture and re-excitation into dots, and radiative or nonradiative recombination rate of the carriers. In figure 1a, at first the carriers are injected to the separate confinement heterostructure (SCH) region, and then they reach the quantum well (QW), after that majority of carriers tunnel to the GS (quantum dot) with probability ε_t. Also the minority carriers escape from the tunnel with probability $1 - \varepsilon_t$ and relax as in the case where the tunnelling is absent. In figure 1b, at first the electrons are injected to SCH, then they go to wetting

layer (WL), after that these carriers are captured to the excited state (ES) in the capture time τ_{ES}^{WL}. Some carriers escape from ES to continuous states in escape time τ_{WL}^{ES}, and the others relax to the ground state (GS) in relaxation time τ_{GS}^{ES}. Also a number of carriers escape from GS to ES in escape time τ_{ES}^{GS}. Therefore, in our model both capture and relaxation of carriers are taken into account for a better description of a realistic lasing process. Thus, based on our model, the rate equations of QD tunnelling injection can be written as follows:

$$\frac{\partial N_S}{\partial t} = \frac{I}{e} - \varepsilon_t \frac{N_S}{\tau_t}(1 - P_{GS}) - (1 - \varepsilon_t)\frac{N_S}{\tau_d} \tag{1}$$

$$\frac{\partial N_{WL}}{\partial t} = (1 - \varepsilon_t)\frac{N_S}{\tau_d} - \frac{N_{WL}}{\tau_{ES}^{WL}}(1 - P_{ES}) + \frac{N_{ES}}{\tau_{WL}^{ES}} - \frac{N_{WL}}{\tau_{WLr}} \tag{2}$$

$$\frac{\partial N_{ES}}{\partial t} = \frac{N_{WL}}{\tau_{ES}^{WL}}(1 - P_{ES}) + \frac{N_{GS}}{\tau_{ES}^{GS}}(1 - P_{ES}) - \frac{N_{ES}}{\tau_{GS}^{ES}}(1 - P_{GS}) - \frac{N_{ES}}{\tau_{WL}^{ES}} - \frac{N_{ES}}{\tau_{ESr}} - \frac{(c/n_r)g_{mES}^1\Gamma}{1 + (\varepsilon_{mES}\Gamma S_{ES}/V_a)}S_{ES} \tag{3}$$

$$\frac{\partial N_{GS}}{\partial t} = \frac{\varepsilon_t N_S}{\tau_t}(1 - P_{GS}) + \frac{N_{ES}}{\tau_{GS}^{ES}}(1 - P_{GS}) - \frac{N_{GS}}{\tau_{ES}^{GS}}(1 - P_{ES}) - \frac{N_{GS}}{\tau_{GSr}} - \frac{(c/n_r)g_{mGS}^1\Gamma}{1 + (\varepsilon_{mGS}\Gamma S_{GS}/V_a)}S_{GS} \tag{4}$$

$$\frac{\partial S_{ES}}{\partial t} = \frac{(c/n_r)g_{mES}^1\Gamma}{1 + (\varepsilon_{mES}\Gamma S_{ES}/V_a)}S_{ES} - \frac{S_{ES}}{\tau_p} + \frac{\beta N_{ES}}{\tau_{sp}} \tag{5}$$

$$\frac{\partial S_{GS}}{\partial t} = \frac{(c/n_r)g_{mGS}^1\Gamma}{1 + (\varepsilon_{mGS}\Gamma S_{GS})/V_a)}S_{GS} - \frac{S_{GS}}{\tau_p} + \frac{\beta N_{GS}}{\tau_{sp}}. \tag{6}$$

In the equations above, N_S, N_{WL}, N_{ES}, and N_{GS} are electron number in SCH, WL, ES, and GS respectively. Also, S_{GS} and S_{ES} are in turn the photon number of GS and ES. I is the injection current. τ_p is the photon lifetime. These equations can be converted to the conventional rate equation of a QD laser when ε_t is zero [22]. g_{mGS}^1 and g_{mES}^1 are the maximum gains in the GS and ES which read as

$$g_{mES}^1 = \frac{2.35\sqrt{2\pi}e^2\hbar}{cn_r\varepsilon_0 m_0^2 V_D}\frac{|P_{cv}^{\delta}|^2}{E_{ES}}\frac{\xi}{\Gamma_{inhom}}(2P_{ES} - 1) \tag{7}$$

$$g_{mGS}^1 = \frac{2.35\sqrt{2\pi}e^2\hbar}{cn_r\varepsilon_0 m_0^2 V_D}\frac{|P_{cv}^{\delta}|^2}{E_{GS}}\frac{\xi}{\Gamma_{inhom}}(2P_{GS} - 1), \tag{8}$$

where V_D is the volume of a dot.

$$V_D = \pi r^2 h. \tag{9}$$

Coverage factor is considered as $\xi = N_d V_D$ in which N_d is the QD volume density. $|P_{cv}^{\sigma}|^2$ is the transition matrix element and is given as follows [20]:

$$|P_{cv}^{\sigma}|^2 = \frac{m_0^2 E_G(E_G + \Delta)}{12m_e(E_G + \frac{2}{3}\Delta)}. \tag{10}$$

Gain compression factor impacts are [20]:

$$\varepsilon_{mES} = \frac{e^2|p_{cv}^{\sigma}|^2\tau_p\hbar}{2n_r^2 m_0^2\varepsilon_0 E_{ES}\Gamma_{hom}} \tag{11}$$

$$\varepsilon_{mGS} = \frac{e^2|p_{cv}^{\sigma}|^2\tau_p\hbar}{2n_r^2 m_0^2\varepsilon_0 E_{GS}\Gamma_{hom}}. \tag{12}$$

The photon lifetime in the cavity τ_p is given as

$$\tau_p^{-1} = \frac{c}{n_r}\left[\alpha_i + \frac{\ln(1/R_1R_2)}{2L_{ca}}\right]. \tag{13}$$

Effective density of states in the WL is

$$\rho_{WL} = \frac{m_e k_B T}{\pi\hbar^2}. \tag{14}$$

τ_{WL}^{ES} is the electron escape time from ES to WL [20]:

$$\tau_{WL}^{ES} = \frac{\tau_{ES}^{WL}\mu_{ES}N_b}{\rho_{WL}(e^{(E_{WL}-E_{ES})}/k_B T)}. \tag{15}$$

τ_{ES}^{GS} is the electron escape time from GS to ES [20]:

$$\tau_{ES}^{GS} = \frac{\tau_{GS}^{ES}\mu_{GS}N_b}{\mu_{ES}(e^{(E_{ES}-E_{GS})}/k_B T)}. \tag{16}$$

P_{ES} and P_{GS} are respectively the occupation probability of electrons in ES and GS,

$$P_{ES} = \frac{N_{ES}}{\mu_{ES}N_d} \tag{17}$$

$$P_{GS} = \frac{N_{GS}}{\mu_{GS}N_d}. \tag{18}$$

Degeneracy of energy state in ES and GS are μ_{ES} and μ_{GS} respectively which are considered 4 and 2 in our model.

The output power is given as

$$P_{out} = \frac{\hbar\omega c S_{GS}\log(1/R_1)}{2n_r L_{ca}}. \tag{19}$$

In the analog modulation, a small AC signal adds to the DC one. So, for a simple case the injection current with modulation frequency ω is $I = I_0 + \Delta I\, e^{j\omega t}$. Here, I_0 is the bias injection current and ΔI is the modulation amplitude. Similar to the injection current, carrier density and photon density can be reformed by small AC signal; $X = X_0 + \Delta X\, e^{j\omega t}$ where $X = N_S$,

N_{WL}, N_{GS}, N_{ES}, S_1 and S_2 are parameters in the relation. Inserting the above time dependence relations to the rate equations and neglecting nanosecond time, we obtain

$$\frac{\partial(N_{s0}+\Delta N_S e^{i\omega t})}{\partial t} = \frac{I_0+\Delta I e^{i\omega t}}{e} - \varepsilon_t \frac{(N_{s0}+\Delta N_S e^{i\omega t})}{\tau_t}\left(1-\frac{(N_{GS}+\Delta N_{GS}e^{i\omega t})}{\mu_{GS}N_D}\right) - (1-\varepsilon_t)\frac{(N_{s0}+\Delta N_S e^{i\omega t})}{\tau_d} \quad (20)$$

and also,

$$\Delta N_S\left(i\omega - \frac{\varepsilon_t}{\tau_t} - \frac{\varepsilon_t N_{GS}}{\tau_t \mu_{GS} N_D}\right) = \frac{\Delta I}{e} + \frac{\varepsilon_t \Delta N_{GS} N_S}{\tau_t \mu_{GS} N_D}. \quad (21)$$

We consider the same formalisms for other carriers and photon and obtain relation for modulation response function $\Delta S_{GS}/\Delta I$. Let us see the values of variables in table 1.

3. Results and discussion

Figures 2a and 2b respectively show the plots of the output power and optical gain respectively as a function of injection current in the presence and absence of tunnelling injection when $\Gamma_{hom} = 10$ meV and $\Gamma_{inhom} = 30$ meV.

As shown in figure 2a, the threshold current for the case with tunnelling is lower than the without tunnelling, but the maximum power in the presence of tunnelling is larger than in the absence of tunnelling. In the absence of tunnelling, by applying injection current, the carriers release their energy with inserting to GS as the thermal energy form. Also, some of them escape to the excited state. So, in the tunnelling case, the cold carriers which tunnel from QW into GS improve the slope efficiency in TIL design. As shown in figure 2b, threshold gain in the case of tunnelling is lower than the case without tunnelling. But the saturated gain in the presence of tunnelling would be more than the case without tunnelling when the injection current is increased.

Figures 3a and 3b indicate the output power and optical gain respectively as a function of injection current in the presence and absence of tunnelling when $\Gamma_{hom} = 10$ meV and $\Gamma_{inhom} = 30$, 40 and 50 meV.

Threshold current for both with tunnelling and without tunnelling is independent of Γ_{inhom}. The output power spectra shown in figure 3a indicate a linear rise with increasing current density, which is followed by an almost constant maximum value at intensified currents. But output power in tunnelling injection reaches

Table 1. Definition of variables which are used in the equations.

Symbol	Description	Value
τ_t	Tunnelling lifetime	0.5 ps
τ_d	Scattering time of SCH	0.5 ps
τ_{WLr}	Carrier non-radiative recombination lifetime in the wetting layer	0.7 ns
τ_{ES}^{WL}	Electron capture time from WL to ES	1 ps
τ_{GS}^{ES}	Electron relaxation time from ES to GS	8 ps
τ_{GSr}	Spontaneous escape lifetime in GS	0.7 ns
τ_{ESr}	Spontaneous escape lifetime in ES	0.7 ns
τ_{sp}	Spontaneous radiation lifetime	0.5 ns
R_1	Right facet reflectivity	30%
R_2	Left facet reflectivity	30%
L_{ca}	Cavity length	900 μm
α_i	Intrinsic absorption coefficient	200 m^{-1}
n_r	Refractive index	3.5
Γ	Optical confinement factor	6%
β	Spontaneous emission coupling coefficient	10^{-4}
r	Radius of a QD (cylindrical shape)	16 nm
h	Height of a QD (cylindrical shape)	16 nm
Δ	Spin–orbit interaction energy of QD mater	0.35 eV
E_{ES}	Recombination energy for ES state	1.0014 eV
E_{GS}	Recombination energy for GS state	0.9644 eV
E_{WL}	Recombination energy for wetting layer	1.0502 eV
E_G	Band gap energy	0.8 eV
ε_t	Tunnelling probability	95%
c	Light speed	3×10^8 m/s
v_g	Group velocity	8.571×10^7 m/s
T	Temperature	293 K
e	Electron charge	1.6×10^{-19} c
$\hbar$	Planck constant	$6.64 \times 10^{-34} m^2$ kg/s
k_B	Boltzmann constant	1.381×10^{-34} J K^{-1}
N_b	Surface density	5×10^{15} m^{-2}
N_d	Volume density	1.5×10^{23} m^{-3}
N_D	Number of dots	1.24×10^7
N_l	Number of layers	5
m_0	Electron mass	9.11×10^{-31} kg
m_e	Effective electron mass in lattice	$0.04 \times m_0$

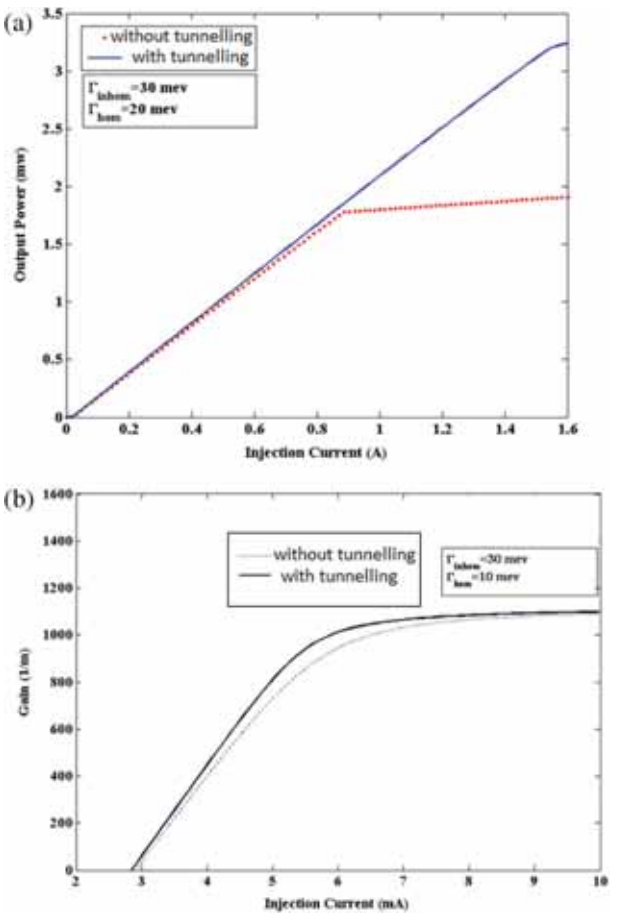

Figure 2. (**a**) Output power vs. current in the presence and absence of tunnelling. Here $\Gamma_{\text{inhom}} = 30$ meV and $\Gamma_{\text{hom}} = 10$ meV and (**b**) optical gain vs. injection current in the presence and absence of tunnelling. Here $\Gamma_{\text{inhom}} = 30$ meV and $\Gamma_{\text{hom}} = 10$ meV.

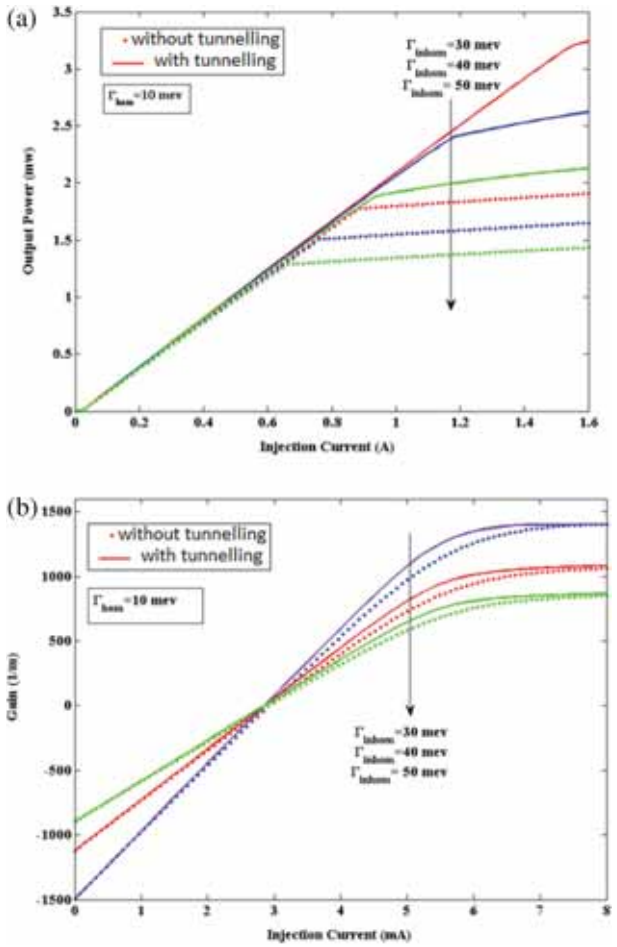

Figure 3. (**a**) Output power vs. injection current with and without tunnelling in various inhomogeneous broadening when $\Gamma_{\text{hom}} = 10$ meV and (**b**) optical gain vs. injection current with and without tunnelling in various inhomogeneous broadening when $\Gamma_{\text{hom}} = 10$ meV.

a maximum in higher injection currents compared to the absence of tunnelling. The best slope efficiency and the enhanced maximum power is viewed for the lowest value of inhomogeneous broadening which is $\Gamma_{\text{inhom}} = 30$ meV and also for the tunnelling case.

As shown in figure 3b, the application of current lower than the threshold current leads to negative optical gain. However, by increasing current up to threshold current (zero gain), the optical gain increases and reaches saturation. The optical gain in the presence of tunnelling is always more than without tunnelling in the high current mode. In the threshold current where the optical gain is zero, the system is independent of Γ_{inhom} for both with tunnelling and without tunnelling conditions. Also, a large saturation gain has been obtained when $\Gamma_{\text{inhom}} = 30$ meV for both with tunnelling and without tunnelling conditions.

Figures 4a–4c show the plots of modulation response function in the presence and absence of tunnelling as a function of frequency for $\Gamma_{\text{hom}} = 10$ meV and for various values of Γ_{inhom}.

From this point of view in figures 4a and 4b, both modulation bandwidth and resonance frequency decrease with increasing Γ_{inhom}, but, the peak amplitude increases with increasing Γ_{inhom}. Our finding is consistent with the results of Gready *et al* [21]. The maximum modulation bandwidth in the presence and absence of tunnelling belongs to almost equal values of Γ_{hom} and Γ_{inhom}. The maximum modulation bandwidths of about 17.8 GHz and 13.9 GHz have been found when $\Gamma_{\text{inhom}} = 20$ meV for the case with tunnelling and without tunnelling respectively. The minimum modulation bandwidths of about 10.4 GHz and 8.9 GHz have been found when $\Gamma_{\text{inhom}} = 50$ meV for the case with tunnelling and without tunnelling respectively. The highest modulation bandwidth is related to the tunnelling case. To explain more we have compared the modulation bandwidth with and without tunnelling for

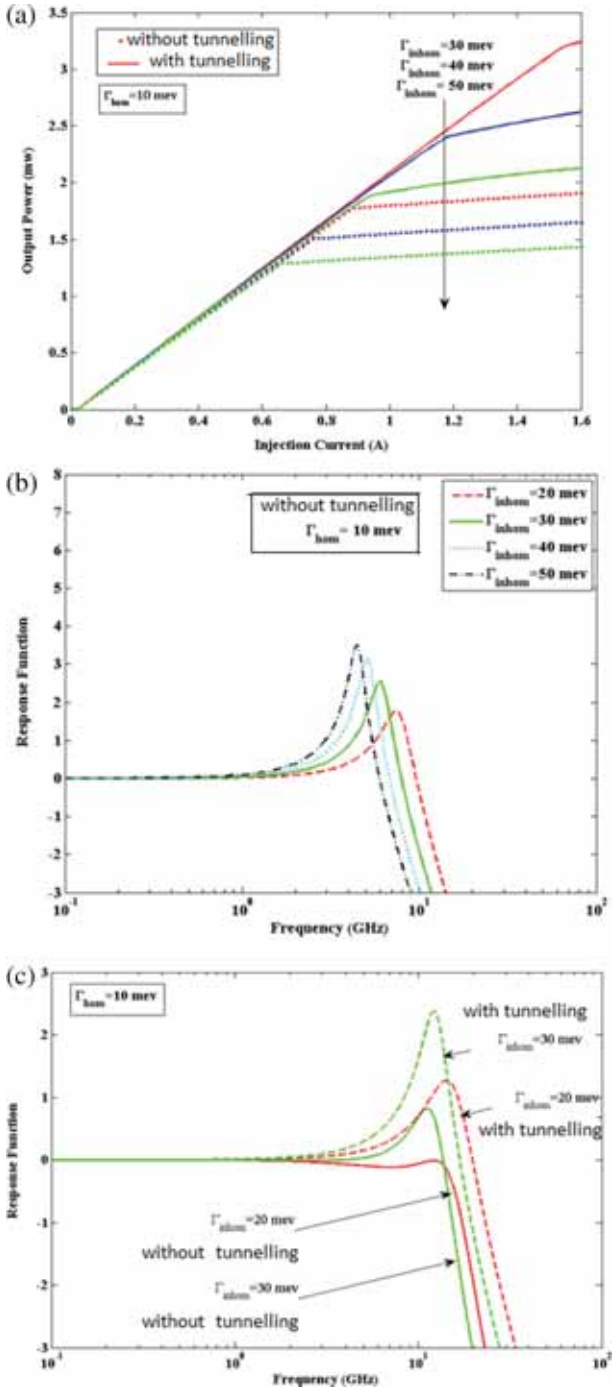

Figure 4. (**a**) Response function frequency with tunnelling in various inhomogeneous broadenings when $\Gamma_{\text{hom}} = 10$ MeV, (**b**) response function frequency without tunnelling in various inhomogeneous broadenings when $\Gamma_{\text{hom}} = 10$ meV and (**c**) response function frequency with and without tunnelling in various inhomogeneous broadenings when $\Gamma_{\text{hom}} = 10$ meV.

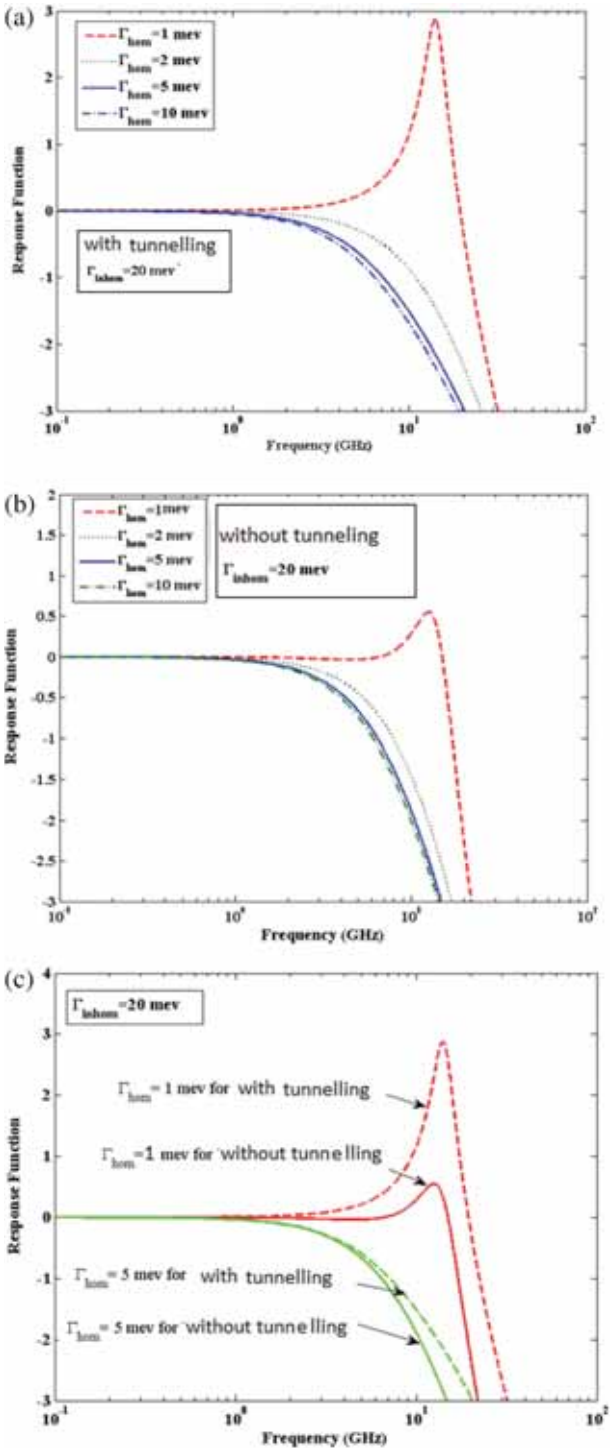

Figure 5. (**a**) Response function frequency with tunnelling in different homogeneous broadenings when $\Gamma_{\text{inhom}} = 20$ meV, (**b**) response function frequency without tunnelling in various homogeneous broadenings when $\Gamma_{\text{inhom}} = 20$ meV and (**c**) response function frequency without and with tunnelling in various homogeneous broadening when $\Gamma_{\text{inhom}} = 20$ meV.

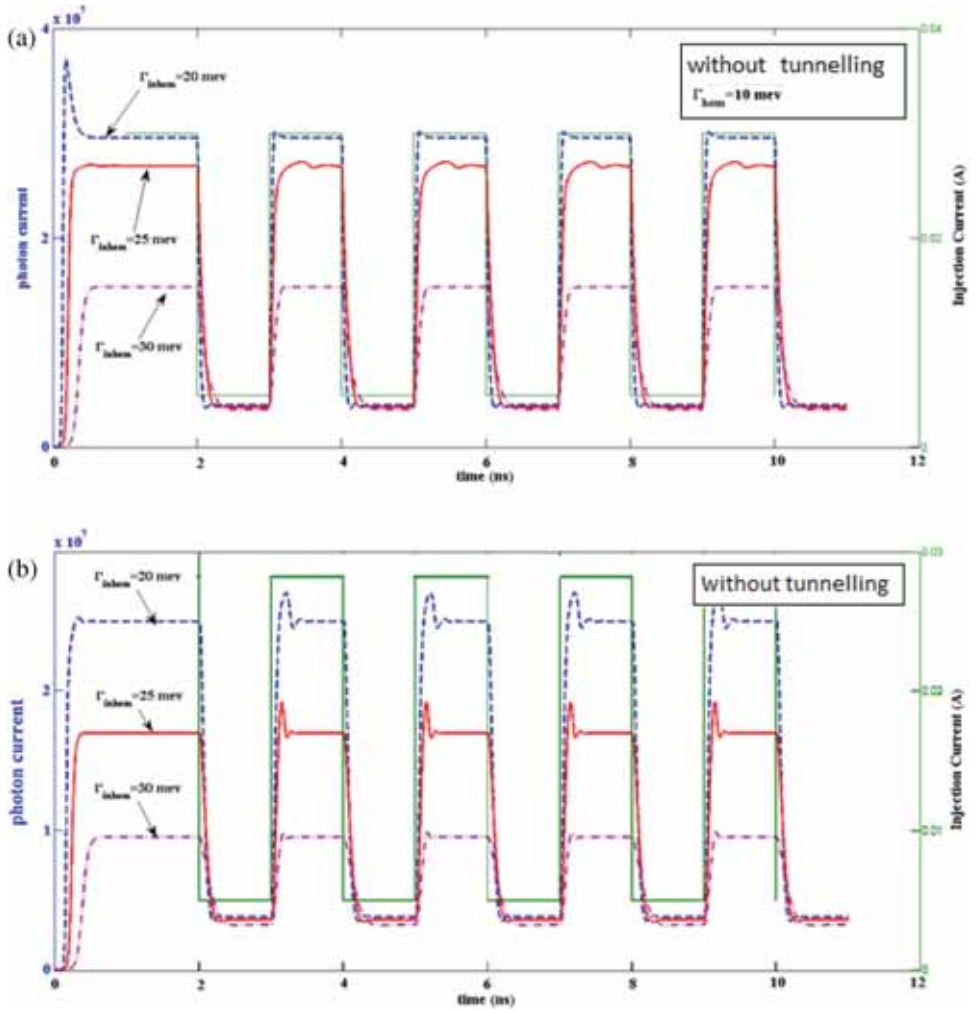

Figure 6. (**a**) Large-signal number of photons and output power for various inhomogeneous broadenings in the presence of tunnelling when $\Gamma_{\text{hom}} = 10$ meV and **(b)** large-signal input current and number of photons for various inhomogeneous broadenings in the absence of tunnelling when $\Gamma_{\text{hom}} = 10$ meV.

$\Gamma_{\text{inhom}} = 20$ meV and 30 meV. Modulation bandwidth, resonance frequency, and the peak amplitude in the presence of tunnelling are more compared to that in the absence of tunnelling.

Figures 5a–5c depict the modulation response function in the presence of tunnelling injection and absence of tunnelling for $\Gamma_{\text{inhom}} = 20$ meV and different values of Γ_{hom}.

As shown in figure 5, modulation bandwidth, peak amplitude, and resonance frequency decrease with increasing Γ_{hom}. In the presence of tunnelling, modulation bandwidth and the peak amplitude are more than that in the absence of tunnelling. Maximum modulation bandwidth is found when $\Gamma_{\text{hom}} = 1$ meV for both cases with tunnelling and without tunnelling and the minimum modulation bandwidth is related to $\Gamma_{\text{hom}} = 10$ meV.

To confirm the importance of inhomogeneous broadening in the application of lasers, we present the output power vs. time curve for AC bias current in the GS state as shown in figure 6. Relaxation oscillation and number of photons reduce by increasing Γ_{inhom} but turn-on delay of the laser extends. In addition, tunnelling into QD region can reduce the relaxation oscillation in the system.

4. Conclusion

To investigate the effect of broadening on the dynamical characteristics and response function, we simulate the QD laser with different broadening parameters. Firstly, we set the full-width at half-maximum (FWHM) of the homogeneous broadening on 10 meV and changed the FWHM of the inhomogeneous width from 20 to 50 meV. Secondly, Γ_{inhom} was set on 30 meV and Γ_{hom} changed from 1 to 10 meV. In general, the relaxation frequency of a laser appeared to be proportional to the differential

gain and the difference between the driving current and the threshold current.

Compared to conventional QD lasers, due to the higher differential gain and lower threshold current of the TIL, it is easier to reach the relaxation frequency even at low driving currents.

In addition, it was shown that carrier transport for the small signal response with and without tunnelling are not the same. For the TIL structure, carrier transport induced parasitic effect which is relatively weak, and modulation bandwidth of TIL is larger than that without tunnelling. Also, these results can be applied to improve the characteristics of light–current diagram, gain, small signal and large signal response of quantum dot lasers.

References

[1] N Kirstädter, N N Ledentsov, M Grundmann, D Bimberg, V M Ustinov, S S Ruvimov, M V Maximov, P S Kop'ev, Zh I Alferov, U Richter, P Werner, U Gösele and J Heydenreich, *Electron. Lett.* **30**, 1416 (1994)
R Mirin, A Gossard and J Bowers, *Electron. Lett.* **32**, 1732 (1996)
N N Ledentsov, M Grundmann, F Heinrichsdorff, D Bimberg, V M Ustinov, A E Zhukov, M V Maximov, Zh I Alferov and J A Lott, *IEEE J. Sel. Top. Quantum Electron.* **6**, 439 (2000)

[2] P Bhattacharya, D Klotzkin, O Qasaimeh, W Zhou, S Krishna and D Zhu, *IEEE J. Sel. Top. Quantum Electron.* **6**, 426 (2000)
L Harris, D J Mowbray, M S Skolnick, M Hopkinson and G Hill, *Appl. Phys. Lett.* **73**, 969 (1998)
P M Smowton, E J Johnston, S V Dewar, P J Hulyer, H D Summers, A Patane, A Polimeni and M Henini, *Appl. Phys. Lett.* **75**, 2169 (1999)
D L Huffaker, G Park, Z Zou, O B Shchekin and D G Deppe, *IEEE J. Sel. Top. Quantum Electron.* **6**, 452 (2000)

[3] M Sugawara, K Mukai, Y Nakata, K Otsubo and H Ishilkawa, *IEEE J. Sel. Top. Quantum Electron.* **6**, 462 (2000)
L F Lester, A Stintz, H Li, T C Newell, E A Pease, B A Fuchs and K J Malloy, *IEEE Photon. Technol. Lett.* **11**, 931 (1999)

[4] D Klotzkin and P Bhattacharya, *J. Lightwave Technol.* **17**, 1634 (1999)

[5] J Faist, F Capasso, D L Sivco, C Sirtori, A L Hutchinson and A Y Cho, *Science* **264**, 553 (1994)

[6] J Faist, F Capasso, C Sirtori, D L Sivco, A L Hutchinson and A Y Cho, *Appl. Phys. Lett.* **66**, 538 (1995)

[7] U Bockelmann and G Bastard, *Phys. Rev. B* **42**, 8947 (1990)

[8] J Urayama, T B Norris, H Jiang, J Singh and P Bhattacharya, *Appl. Phys. Lett.* **80**, 2162 (2002)

[9] K Kim, J Urayama, T B Norris, J Singh, J Phillips and P Bhattacharya, *Appl. Phys. Lett.* **81**, 670 (2002)

[10] J Urayama, T Norris, J Singh and P Bhattacharya, *Phys. Rev. Lett.* **86**, 4930 (2001)

[11] H C Wong, G B Ren and J M Rorison, *IEEE Photon. Technol. Lett*. **18**, 2075 (2006)

[12] H Taleb and K Abedi, *Optoelectron.* **5**, 445 (2012)

[13] S W Chang, S L Chuang and N Holonyak, Jr, *Phys. Rev. B* **70**, 125312 (2004)

[14] P Bhattacharya and S Ghosh, *Appl. Phys. Lett.* **80**, 3482 (2002)

[15] W Rudno-Rudziński, G Sek, K Ryczko, M Syperek, J Misiewicz, E S Semenova, A Lemaitre and A Ramdane, *Appl. Phys. Lett.* **94**, 171906 (2009)

[16] C Meuer, J Kim, M Lammlin, S Liebich, G Eisenstein, R Bonk, T Vallaitis, J Leuthold, A Kovsh, I Kresnikov and D Bimberg, *IEEE J. Sel. Top. Quantum Electron.* **15**, 749 (2009)

[17] Y Matsumoto, T Wamura and A Iwaki, *Appl. Phys. Lett.* **55**, 2535 (1989)

[18] M Sugawara, N Hatori, H Ebe, Y Arakawa, T Akiyama, K Otsubo and Y Nakata, *J. Appl. Phys.* **97**, 043523 (2005)

[19] O Qasaimeh and H Khanfar, *IEE Proc.-Optoelectron.* **151**, 143 (2004)

[20] M Sugawara, *Self-assembled InGaAs/GaAs quantum dots* (Academic Press, 1999) Vol. 60

[21] D Gready and G Eisenstein, *IEEE J. Quantum Electron.* **47**(**7**), 944 (2011)

[22] A Fali, E Rajaei and Z Danesh Kaftroudi, *J. Korean Phys. Soc.* **64**(**1**), 16 (2014)